Article

Periodic activity from a fast radio burst source

https://doi.org/10.1038/s41586-020-2398-2

Received: 23 January 2020

Accepted: 28 April 2020

Published online: 17 June 2020

Check for updates

The CHIME/FRB Collaboration*

Fast radio bursts (FRBs) are bright, millisecond-duration radio transients originating from sources at extragalactic distances[1], the origin of which is unknown. Some FRB sources emit repeat bursts, ruling out cataclysmic origins for those events[2–4]. Despite searches for periodicity in repeat burst arrival times on timescales from milliseconds to many days[2,5–7], these bursts have hitherto been observed to appear sporadically and—although clustered[8]—without a regular pattern. Here we report observations of a 16.35 ± 0.15 day periodicity (or possibly a higher-frequency alias of that periodicity) from the repeating FRB 180916.J0158+65 detected by the Canadian Hydrogen Intensity Mapping Experiment Fast Radio Burst Project[4,9]. In 38 bursts recorded from 16 September 2018 to 4 February 2020 UTC, we find that all bursts arrive in a five-day phase window, and 50 per cent of the bursts arrive in a 0.6-day phase window. Our results suggest a mechanism for periodic modulation either of the burst emission itself or through external amplification or absorption, and disfavour models invoking purely sporadic processes.

In 2019 the Canadian Hydrogen Intensity Mapping Experiment Fast Radio Burst Project (CHIME/FRB) collaboration reported the discovery of eight repeating FRB sources[4], including FRB 180916.J0158+65, which was recently localized to a star-forming region in a nearby massive spiral galaxy at redshift 0.0337 ± 0.0002 (ref. [10]). From September 2018 to February 2020, the CHIME telescope FRB back end detected a total of 38 bursts from FRB 180916.J0158+65, which is the most active source in the published CHIME/FRB sample. The barycentric arrival times for the 38 bursts (including those that have been published before) from FRB 180916.J0158+65, corrected for delays from the dispersion measure (DM) of the pulse are listed in Extended Data Table 1.

To search for periodicity, the burst arrival times (spanning a 500-d range) were folded with different periods from 1.5 to 100 d (see Methods), with a Pearson's χ^2 test applied to resulting profiles created with different numbers of phase bins[11]. A reduced $\chi^2 \gg 1$ with respect to a uniform distribution indicates a periodicity unlikely to arise by chance. Furthermore, to account for possible non-Poissonian statistics of the bursts[8], we conducted the search with weighting schemes that considered clustered bursts of different time ranges to be correlated events (see Methods).

Searches with different weightings return periodograms of similar shape and have the same primary peak with significance varying between 4.5–10σ. As an example, the reduced χ^2 versus the period with five phase bins, using a weighting that counts only active days instead of individual events, is shown in Fig. 1a. A distinct peak is detected at 16.35 ± 0.15 d, with a probability of chance occurrence of about 10^{-7} (equivalent to 5σ), accounting for the number of independent periods searched. The other χ^2 peaks correspond to harmonics and subharmonics of the period; the peak at 32.7 d is the next most prominent. As a check, the same procedure was run on two types of control samples: (1) a mock dataset, consisting of burst arrival times randomly sampled according to the daily exposure of FRB 180916.J0158+65 with the full width at half maximum (FWHM) of the synthesized beams of CHIME/FRB at 600 MHz (Fig. 1b); and (2) randomly selected pulses from Galactic radio pulsars of similar declination detected by CHIME/FRB (Fig. 1c), which have the same limited daily exposure and long-term sensitivity changes as the data for FRB 180916.J0158+65. The 16.35-d periodicity is absent in the control samples, and with 10^6 sets of control samples of each type, no other periods have reached the level of significance of the 16.35-d period for FRB 180916.J0158+65 by chance.

Alternative search methods—such as folding the events and evaluating the resulting profiles with multinomial distribution, using the H test[12] and applying discrete Fourier transform searches with incoherent harmonic summing[13]—also return the 16.35-d period, with nominal significances between 4 and 13σ under various assumptions (see Methods). Figure 2 shows the arrival times of the bursts from FRB 180916.J0158+65 from 28 August 2018 to 4 February 2020, together with the daily exposure to the source and instrument sensitivity. The instrument was operating for the majority of this time interval with nominal sensitivity; however, the bursts are detected only in a narrow interval at the reported periodicity. Note that the short regular daily exposure of CHIME leads to a degeneracy between specific periods of the order of hours to a day and the 16.35-d period (see Methods). Nevertheless, the statistical significance of an astrophysical periodicity remains unaffected. A modest amount of data with bursts detected outside the CHIME observing windows may be able to determine the true period. We conclude that this is the first detected periodicity of any kind in an FRB source.

In addition to the CHIME/FRB detections, FRB 180916.J0158+65 was detected by the European Very-long-baseline-interferometry Network (EVN) during 3.5 h of exposure on 19 June 2019 at a central frequency of 1.7 GHz (ref. [10].). The arrival times of the EVN detection appear at the

*A list of authors and their affiliations appears at the end of the paper.

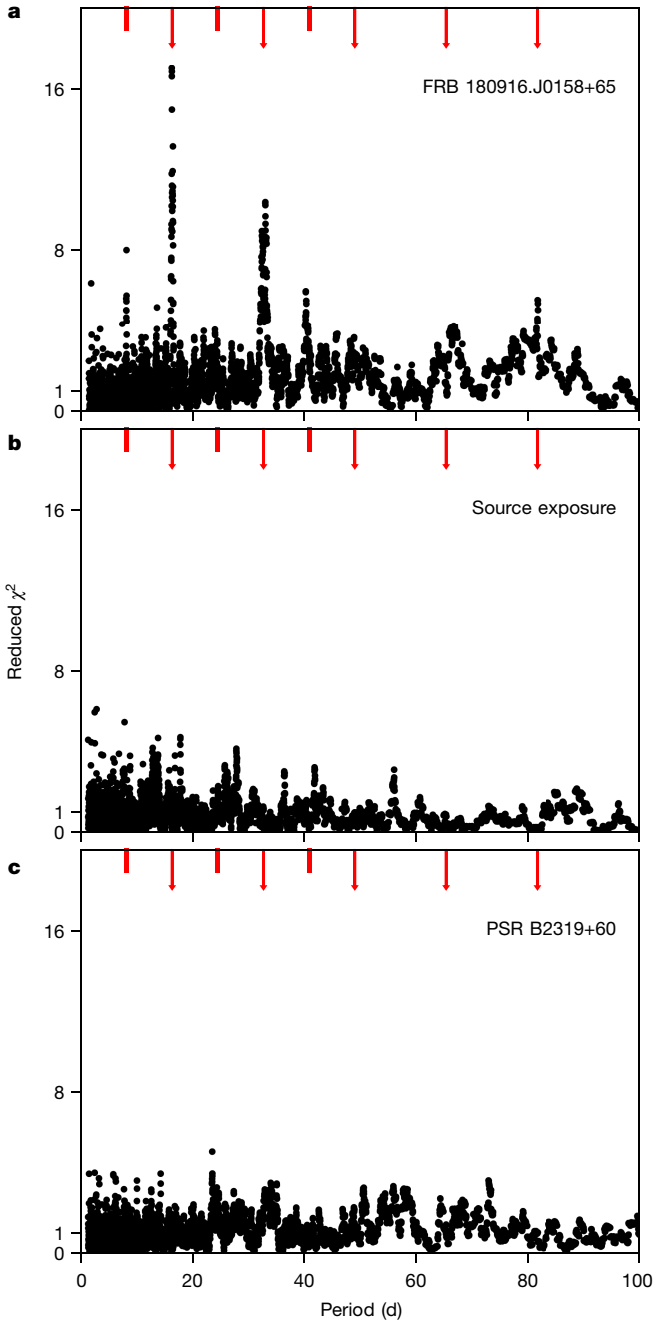

Fig. 1 | Periodograms of FRB 180916.J0158+65 and control samples. **a**, Reduced χ^2 periodogram with respect to a uniform distribution of burst arrival times for different folding periods for FRB 180916.J0158+65, detected by CHIME/FRB. Only bursts separated by a sidereal day are considered independent in this approach. Periods close to the first five subharmonics of a sidereal day are avoided. Details of the calculation of χ^2 and other approaches are presented in Methods. **b**, Periodogram of arrival times of mock bursts, randomly sampled according to the daily exposure to FRB 180916.J0158+65 within the FWHM of the synthesized beams of CHIME/FRB at 600 MHz. **c**, Periodogram of randomly selected pulses of the Galactic radio pulsar B2319+60 detected by the same instrument and software. In **a**–**c**, the arrows indicate the first five subharmonics of the 16.35-d periodicity and the vertical lines mark the harmonics of half a period.

leading edge of the active phase determined from an analysis of CHIME/FRB timing data at lower frequencies of 400–800 MHz (Figs. 2, 3). Subsequently, however, during a predicted epoch of peak activity (29 October 2019 and 30 October 2019), we made observations towards the direction of FRB 180916.J0158+65 for 17.6 h using the 100-m Effelsberg telescope at 1.4 GHz (see Methods). In that search, we did not detect any bursts above a fluence limit of 0.17 Jy ms (for bursts with widths of 1 ms and a signal-to-noise (S/N) threshold of 7σ). The Effelsberg telescope observations were contemporaneous with two CHIME/FRB-detected bursts from FRB 180916.J0158+65. Future multi-frequency radio observations of FRB 180916.J0158+65 will aid in understanding the relationship between burst activity and emission frequency.

We estimate the detection rate of the CHIME/FRB system to be $0.9^{+0.5}_{-0.4}$ bursts per hour above a fluence threshold of 5.2 Jy ms for a ±2.7-d interval around each epoch of activity. Additionally, we estimate the detection rate for three subintervals in the active phase. We find the rate in a ±0.9-d subinterval centred at the epoch of peak activity to be inconsistent with that estimated for the subinterval most separated from the epoch of peak activity, suggesting that burst activity is not constant within the active phase (see Methods). Poissonian uncertainties associated with all rate measurements are at the 95% confidence level and the fluence thresholds are complete to the 90% confidence level. The 95% confidence upper limit on the detection rate during inactive phases with non-zero exposure is 0.07 bursts per hour above a fluence threshold of 5.1 Jy ms.

Figure 3 shows the burst fluence and DM as a function of phase. The phase is computed by folding burst arrival times at a period of 16.35 d with modified Julian date (MJD) 58369.18 referenced as phase 0. Using this definition, phase 0.5 corresponds to the mean of the folded arrival times. There is no apparent trend of burst fluence with phase in the 400–800 MHz band. The best-fit DMs of four CHIME/FRB bursts with high-time-resolution data (marked red), as well as the DM of the brightest burst detected by the EVN[10] (which is accurately determined owing to the narrowness of the burst), are consistent with each other, constraining changes in the DM to be <0.1 pc cm^{-3}. These bursts are detected over a time span of about 176 d, which strongly constrains any potential DM variation within this time period. The DMs of the other bursts—although possibly subject to important biases (see Methods)—disfavour DM changes greater than 2 pc cm^{-3} over the full 400-d span of the events. In summary, there is no obvious phase- or time-related change in DM in the current data.

Bursts from FRB 180916.J0158+65 and other repeating FRB sources display complex morphological features[14]: they tend to exhibit a bandwidth of 100–200 MHz at different central frequencies, with temporal widths of a few milliseconds to tens of milliseconds. Some exhibit downward-drifting sub-bursts at a few to tens of megahertz per millisecond in the CHIME band[4], up to almost a gigahertz per millisecond at 6.5 GHz in the case of FRB 121102[14,15]. We observe no trend in the burst temporal width or bandwidth for detections of FRB 180916.J0158+65 detections by CHIME/FRB thus far—neither as a function of time nor phase. Moreover, drifting sub-bursts appear to occur at all phases. In fact, when dedispersed to the average best-fit DM from high-resolution baseband data (as in Extended Data Fig. 1, 2) nearly all bursts seem to exhibit downward-drifting sub-bursts.

The discovery of a periodicity in a repeating FRB source is an important clue to the nature of this object. Models in which the emission is purely sporadic (for example, giant pulses as seen from the Crab pulsar[16] or from an isolated young magnetar[17–19]; see below), are excluded for this source. One possible explanation for periodicity is orbital motion, where the emitter is perhaps a neutron star, which could be a radio pulsar or magnetar. Neutron stars are commonly found in binary systems with stellar, substellar or compact companions. Massive O- and B-type companion stars to neutron stars have been observed, generally in eccentric orbits of many days to months[20]. The narrow duty cycle for bursting in the FRB 180916.J0158+65 system, assuming a 16.35-d period, could be related to eccentricity. The periodicity could reflect phase-related emission (for example, through an interaction with the outflow[21,22] or asteroid belt[23] of the companion).

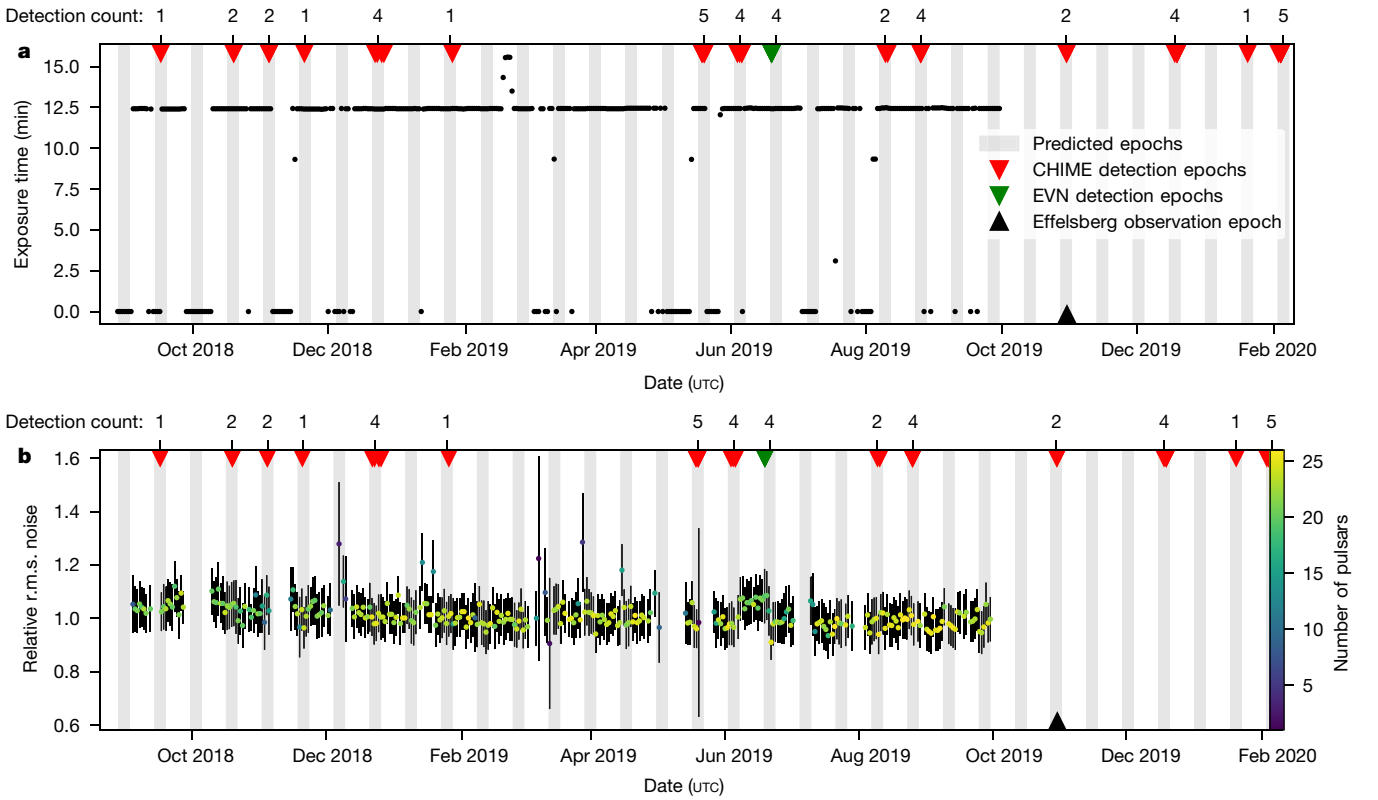

Fig. 2 | Timeline of the daily exposure of CHIME/FRB to FRB 180916.J0158+65. Downward triangle markers on the top axis indicate arrival times for detections with CHIME/FRB or EVN; the number of detections in each active phase is indicated above the markers. The upward triangle marker on the bottom axis indicates the epoch of non-detection of the source by the Effelsberg telescope. The grey shaded regions show a ±2.7-d interval around the estimated epochs of source activity. **a**, The exposure to the source within the FWHM of the synthesized beams at 600 MHz is shown in black. We truncate our reported exposure on 30 September 2019 owing to an upgrade of the software (see Methods). **b**, The variation in the daily relative root mean square (r.m.s.) noise at the position of FRB 180916.J0158+65, depicted as coloured points with 1σ uncertainties, measured using a collection of pulsars detected by CHIME/FRB. There is clearly substantial exposure and nominal sensitivity to the source well outside the regions of observed activity.

The periodicity could also reflect a reduction in effective radio opacity at apastron, where the radio bursts do not pass through the companion wind or disk[20,21]. Bursts could also be lensed by companion wind clumps or disk material near periastron[24]—but if so, the preference for a downward-drifting frequency structure is puzzling (see Fig. 2). With a companion casting material in the orbit, phase-dependent DM or rotation measure variations could eventually be observed, especially with wideband or lower-frequency observations. Periodic variation could also arise from classical binary precession, which is seen in some stellar–neutron star binaries[25]. In Galactic binaries composed of a massive star and a pulsar, bright X-ray and γ-ray emission can be observed[26]; if detected in this system, such emission would be a strong diagnostic (but the 149-Mpc distance[10] here will make a detection challenging). A compact-object companion to the emitter is also possible. Given the location[10] of the source in the outskirts of a massive spiral galaxy, a supermassive black hole companion seems unlikely; however, an intermediate- or stellar-mass black hole companion is possible and could result in periodically observed bursts if there is relativistic orbital precession.

Isolated compact-object scenarios may present challenges. One popular model used to explain repeating FRBs invokes a magnetar central engine[17–19]. A periodicity could arise from the rotation of such a star. However, known Galactic magnetars[27] have rotation periods <12 s. One young 6.67-h X-ray pulsar has been argued to be a magnetar[28], that has been spun down by torque from a disk of material. However, simulations of such 'fallback disks'[29] suggest it is difficult to produce periodicities of several hours (the timescale of possible aliased periods), let alone several weeks. A handful of known radio pulsars show intermittent, quasi-periodic emission intervals with periods of several days, and which are known to be magnetospheric in origin[30] (though otherwise poorly understood). However, the radio luminosities of those sources are at least nine orders of magnitude lower than that of FRB 180916.J0158+65 and all other FRB sources. Long-term precession in an isolated spinning pulsar could modulate the visibility of bright bursts produced through an exotic mechanism. However, long-lived precession in isolated neutron stars has been thought to be impossible because of rapid damping owing to superfluid-vortex-line pinning in the stellar interior[31]—more recent work[32,33] incorporates modifications to the superfluid properties and may allow for precession. If the source were precessing, the bursts would probably be emerging from a fixed region on the star—probably a magnetic pole—and the 30% active phase of the source would suggest either a small viewing angle or a large polar region, possibilities that may be distinguishable using observations of the variation of the position angle of linearly polarized emission.

To test for an aliased periodicity, we encourage observations with exposure functions different from those of CHIME. Future observations, both intensity and polarimetric and at all wavebands, could distinguish among the proposed models, and the generality of the phenomenon may be determined by searches for periodicities in other repeaters.

Online content

Any methods, additional references, Nature Research reporting summaries, source data, extended data, supplementary information,

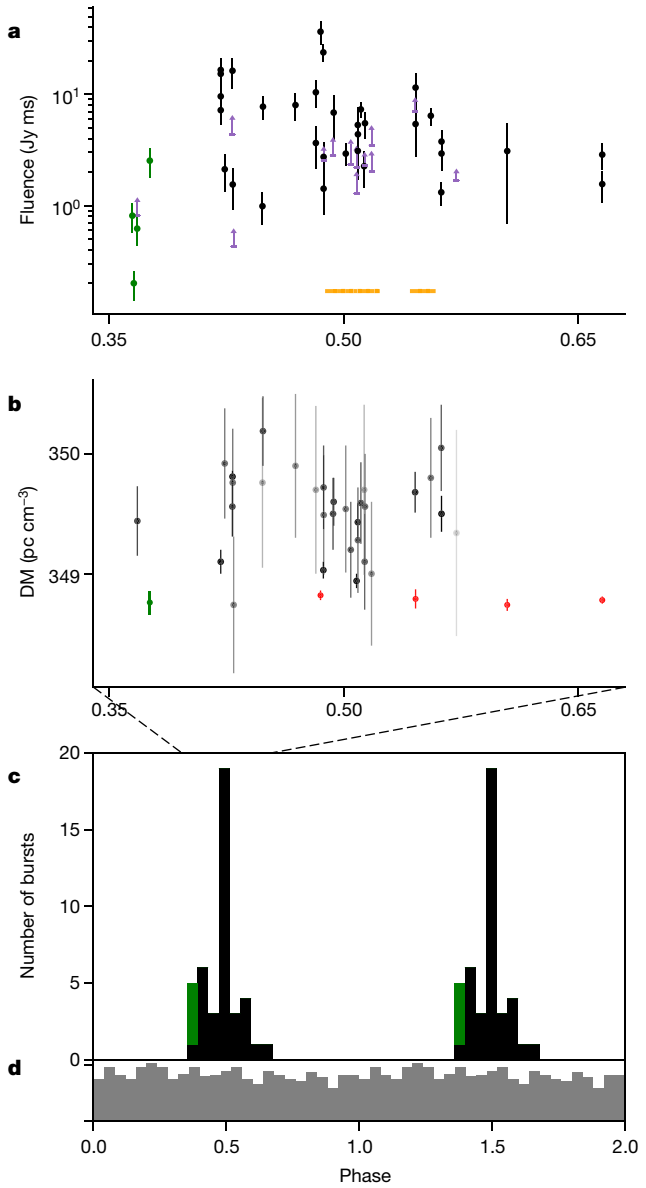

Fig. 3 | Burst properties against phase. FRB 180916.J0158+65 bursts folded at the 16.35-d period with MJD 58369.18 referenced as phase 0. The parameters from 1.7-GHz EVN detection are in green. **a**, Fluence versus phase. Purple arrows indicate the lower bounds derived from CHIME detections; orange lines are the fluence threshold for 1-ms bursts for the search in the 1.4-GHz Effelsberg telescope data. Error bars on the CHIME detections represent the average fluence uncertainty estimated from known point-source transits. **b**, DM versus phase, with 1σ error bars. DMs derived from high-resolution baseband data from CHIME/FRB are in red. DMs from CHIME/FRB intensity data are in black; these are subject to potential biases (see Methods). Data points with larger errors are displayed with higher transparency. **c**, Number of bursts at each phase; as in **a** and **b**, the EVN detection data are in green. **d**, Relative exposure time of different phase bins to FRB 180916.J0158+65 within the FWHM of the CHIME synthesized beams at 600 MHz.

acknowledgements, peer review information; details of author contributions and competing interests; and statements of data and code availability are available at https://doi.org/10.1038/s41586-020-2398-2.

1. Lorimer, D. R., Bailes, M., McLaughlin, M. A., Narkevic, D. J. & Crawford, F. A bright millisecond radio burst of extragalactic origin. *Science* **318**, 777–780 (2007).
2. Spitler, L. G. et al. A repeating fast radio burst. *Nature* **531**, 202–205 (2016).
3. The CHIME/FRB Collaboration. A second source of repeating fast radio bursts. *Nature* **566**, 235–238 (2019).
4. The CHIME/FRB Collaboration. CHIME/FRB detection of eight new repeating fast radio burst sources. *Astrophys. J. Lett.* **885**, 24 (2019).
5. Scholz, P. et al. The repeating fast radio burst FRB 121102: multi-wavelength observations and additional bursts. *Astrophys. J.* **833**, 177 (2016).
6. Zhang, Y. G. et al. Fast radio burst 121102 pulse detection and periodicity: a machine learning approach. *Astrophys. J.* **866**, 149 (2018).
7. Gourdji, K. et al. A sample of low-energy bursts from FRB 121102. *Astrophys. J. Lett.* **877**, 19 (2019).
8. Oppermann, N., Yu, H.-R. & Pen, U.-L. On the non-Poissonian repetition pattern of FRB121102. *Mon. Not. R. Astron. Soc.* **475**, 5109–5115 (2018).
9. The CHIME/FRB Collaboration. The CHIME Fast Radio Burst Project: system overview. *Astrophys. J.* **863**, 48 (2018).
10. Marcote, B. et al. A repeating fast radio burst source localized to a nearby spiral galaxy. *Nature* **577**, 190–194 (2020).
11. Leahy, D. A. et al. On searches for pulsed emission with application to four globular cluster X-ray sources: NGC 1851, 6441, 6624 and 6712. *Astrophys. J.* **266**, 160–170 (1983).
12. de Jager, O. C., Raubenheimer, B. C. & Swanepoel, J. W. H. A powerful test for weak periodic signals with unknown light curve shape in sparse data. *Astron. Astrophys.* **221**, 180–190 (1989).
13. Ransom, S. M., Eikenberry, S. S. & Middleditch, J. Fourier techniques for very long astrophysical time-series analysis. *Astron. J.* **124**, 1788–1809 (2002).
14. Hessels, J. W. T. et al. FRB 121102 bursts show complex time-frequency structure. *Astrophys. J. Lett.* **876**, 23 (2019).
15. Josephy, A. et al. CHIME/FRB detection of the original repeating fast radio burst source FRB 121102. *Astrophys. J. Lett.* **882**, 18 (2019).
16. Lyutikov, M., Burzawa, L. & Popov, S. B. Fast radio bursts as giant pulses from young rapidly rotating pulsars. *Mon. Not. R. Astron. Soc.* **462**, 941–950 (2016).
17. Lyubarsky, Y. A model for fast extragalactic radio bursts. *Mon. Not. R. Astron. Soc.* **442**, L9–L13 (2014).
18. Beloborodov, A. M. A flaring magnetar in FRB 121102? *Astrophys. J. Lett.* **843**, 26 (2017).
19. Metzger, B. D., Margalit, B. & Sironi, L. Fast radio bursts as synchrotron maser emission from decelerating relativistic blast waves. *Mon. Not. R. Astron. Soc.* **485**, 4091–4106 (2019).
20. Johnston, S. et al. PSR 1259 63: a binary radio pulsar with a Be star companion. *Astrophys. J.* **387**, L37–L41 (1992).
21. Mottez, F. & Zarka, P. Radio emissions from pulsar companions: a refutable explanation for galactic transients and fast radio bursts. *Astron. Astrophys.* **569**, A86 (2014).
22. Zhang, B. FRB 121102: a repeatedly combed neutron star by a nearby low-luminosity accreting supermassive black hole. *Astrophys. J. Lett.* **854**, 21 (2018).
23. Dai, Z. G., Wang, J. S., Wu, X. F. & Huang, Y. F. Repeating fast radio bursts from highly magnetized pulsars traveling through asteroid belts. *Astrophys. J.* **829**, 27 (2016).
24. Main, R. et al. Pulsar emission amplified and resolved by plasma lensing in an eclipsing binary. *Nature* **557**, 522–525 (2018).
25. Kaspi, V. M., Bailes, M., Manchester, R. N., Stappers, B. W. & Bell, J. F. Evidence from a precessing pulsar orbit for a neutron-star birth kick. *Nature* **381**, 584–586 (1996).
26. Chernyakova, M. et al. Multi-wavelength observations of the binary system PSR B1259–63/LS 2883 around the 2014 periastron passage. *Mon. Not. R. Astron. Soc.* **454**, 1358–1370 (2015).
27. Olausen, S. A. & Kaspi, V. M. The McGill Magnetar Catalog. *Astrophys. J. Suppl.* **212**, 6 (2014).
28. D'Ai, A. et al. Evidence for the magnetar nature of 1E 161348–5055 in RCW 103. *Mon. Not. R. Astron. Soc.* **463**, 2394–2404 (2016).
29. Xu, K. & Li, X.-D. On the fallback disk around the slowest isolated pulsar, 1E 161348–5055. *Astrophys. J.* **877**, 138 (2019).
30. Kramer, M., Lyne, A. G., O'Brien, J. T., Jordan, C. A. & Lorimer, D. R. A periodically active pulsar giving insight into magnetospheric physics. *Science* **312**, 549–551 (2006).
31. Shaham, J. Free precession of neutron stars: role of possible vortex pinning. *Astrophys. J.* **214**, 251–260 (1977).
32. Akgün, T., Link, B. & Wasserman, I. Precession of the isolated neutron star PSR B1828–11. *Mon. Not. R. Astron. Soc.* **365**, 653–672 (2006).
33. Goglichidze, O. A. & Barsukov, D. P. A possible way to reconcile long-period precession with vortex pinning in neutron stars. *Mon. Not. R. Astron. Soc.* **482**, 3032–3044 (2019).

The CHIME/FRB Collaboration

M. Amiri[1], B. C. Andersen[2,3], K. M. Bandura[4,5], M. Bhardwaj[2,3], P. J. Boyle[2,3], C. Brar[2,3], P. Chawla[2,3], T. Chen[6], J. F. Cliche[2,3], D. Cubranic[1], M. Deng[1], N. T. Denman[7], M. Dobbs[2,3], F. Q. Dong[1], M. Fandino[1], E. Fonseca[2,3], B. M. Gaensler[8,9], U. Giri[10,11], D. C. Good[1], M. Halpern[1], J. W. T. Hessels[12,13], A. S. Hill[14,15], C. Höfer[1], A. Josephy[2,3], J. W. Kania[16], R. Karuppusamy[17], V. M. Kaspi[2,3], A. Keimpema[18], F. Kirsten[19], T. L. Landecker[15], D. A. Lang[10,11], C. Leung[6,20], D. Z. Li[8,17,21,22]✉, H.-H. Lin[17,21], B. Marcote[18], K. W. Masui[6,20], R. Mckinven[8,9], J. Mena-Parra[6], M. Merryfield[2,3], D. Michilli[2,3], N. Milutinovic[1,15], A. Mirhosseini[1], A. Naidu[2,3], L. B. Newburgh[23], C. Ng[8], K. Nimmo[12,13], Z. Paragi[18], C. Patel[2,3,8], U.-L. Pen[8,10,17,21,24], T. Pinsonneault-Marotte[1], Z. Pleunis[2,3], M. Rafiei-Ravandi[10], M. Rahman[8], S. M. Ransom[25], A. Renard[8], P. Sanghavi[4,5], P. Scholz[8,15], J. R. Shaw[1], K. Shin[6,20], S. R. Siegel[2,3], S. Singh[2,3], R. J. Smegal[1], K. M. Smith[10], I. H. Stairs[1], S. P. Tendulkar[2,3], I. Tretyakov[8,22], K. Vanderlinde[8,9], H. Wang[6,20], X. Wang[26], D. Wulf[2,3], P. Yadav[1] & A. V. Zwaniga[2,3]

[1]Department of Physics and Astronomy, University of British Columbia, Vancouver, British Columbia, Canada. [2]Department of Physics, McGill University, Montreal, Quebec, Canada. [3]McGill Space Institute, McGill University, Montreal, Quebec, Canada. [4]CSEE, West Virginia University, Morgantown, WV, USA. [5]Center for Gravitational Waves and Cosmology, West Virginia University, Morgantown, WV, USA. [6]MIT Kavli Institute for Astrophysics and Space Research, Massachusetts Institute of Technology, Cambridge, MA, USA. [7]Central Development Laboratory, National Radio Astronomy Observatory, Charlottesville, VA, USA. [8]Dunlap Institute for Astronomy and Astrophysics, University of Toronto, Toronto, Ontario, Canada. [9]David A. Dunlap Department of Astronomy and Astrophysics, University of Toronto, Toronto, Ontario, Canada. [10]Perimeter Institute for Theoretical Physics, Waterloo, Ontario, Canada. [11]Department of Physics and Astronomy, University of Waterloo, Waterloo, Ontario, Canada. [12]ASTRON, Netherlands Institute for Radio Astronomy, Dwingeloo, The Netherlands. [13]Anton Pannekoek Institute for Astronomy, University of Amsterdam, Amsterdam, The Netherlands. [14]Department of Computer Science, Math, Physics, and Statistics, University of British Columbia, Kelowna, British Columbia, Canada. [15]Dominion Radio Astrophysical Observatory, Herzberg Research Centre for Astronomy and Astrophysics, National Research Council Canada, Penticton, British Columbia, Canada. [16]Department of Physics and Astronomy, West Virginia University, Morgantown, WV, USA. [17]Max Planck Institute for Radio Astronomy, Bonn, Germany. [18]Joint Institute for VLBI ERIC (JIVE), Dwingeloo, The Netherlands. [19]Department of Space, Earth and Environment, Chalmers University of Technology, Onsala Space Observatory, Onsala, Sweden. [20]Department of Physics, Massachusetts Institute of Technology, Cambridge, MA, USA. [21]Canadian Institute for Theoretical Astrophysics, Toronto, Ontario, Canada. [22]Department of Physics, University of Toronto, Toronto, Ontario, Canada. [23]Department of Physics, Yale University, New Haven, CT, USA. [24]CIFAR Program in Gravitation and Cosmology, Canadian Institute for Advanced Research, Toronto, Ontario, Canada. [25]National Radio Astronomy Observatory, Charlottesville, VA, USA. [26]School of Physics and Astronomy, Sun Yat-sen University, Zhuhai, China. ✉e-mail: dzli@cita.utoronto.ca

Methods

Burst characterization

Burst DMs and models of dynamic spectra were determined in a manner similar to that used for earlier detections of the source[3]. In summary, bursts were dedispersed to a fiducial DM = 349.75 pc cm^{-3} and their DMs were subsequently optimized to maximize structure by calculating the phase coherence of emission in all frequency channels with the DM phase package[34](Seymour et al., manuscript in preparation) over a range of trial DMs. The alignment of sub-bursts in burst dynamic spectra was verified by eye and best-fit values are listed in Extended Data Table 1.

In addition, we fit structure-optimizing DMs using the same method for four FRB 180916.J0158+65 bursts for which complex voltage (baseband) data were saved to disk: the 181225 and 181226 bursts presented previously, and the 190604 burst and second 190605 burst presented in this work. The baseband system has a 2.56-μs time resolution and 0.390625-MHz frequency resolution, but we downsampled the data in time to 40.96, 40.96, 20.48 and 81.92 μs, for the four bursts respectively, to optimize *S*/*N* and resolution. We find that DMs of 348.78 ± 0.02, 348.82 ± 0.02, 348.82 ± 0.05 and 348.86 ± 0.05 pc cm^{-3}, respectively, best align the substructures in the four bursts. We note that the DMs from CHIME/FRB intensity data, which have 0.98304-ms time resolution, are biased high if a burst is comprised of unresolved downward-drifting sub-bursts that only become obvious at higher time resolution. As the DMs fitted at high time resolution are all consistent with one average DM = 348.82 pc cm^{-3} (which is also consistent with the DM of the brightest burst detected by the EVN), we use that value to dedisperse intensity data for visualization of the millisecond-resolution data.

Dynamic spectra of the intensity data (at millisecond resolution) for the 27 newly published bursts presented in this work are shown in Extended Data Fig. 1, 2; and dynamic spectra for the four bursts for which the baseband data (at a time resolution of few tens of microseconds) were analysed are shown in Extended Data Fig. 3.

Single- or multi-component models of dynamic spectra were fit to millisecond-resolution total-intensity data acquired for each burst using a least-squares algorithm[35]. We applied two-dimensional models of spectra that consisted of Gaussian temporal shapes and either Gaussian or weighted power-law spectral energy distributions. Owing to the complex and varying structure of bursts from this source, we report best-fit parameters using models that do not explicitly fit for one-sided scattering tails, and thus yield estimates of 'observed' widths. Best-fit observed widths and burst arrival times, referenced to the Solar System barycentre and infinite frequency using per-burst DMs and the EVN position for this source are presented in Extended Data Table 1.

Three CHIME/FRB events from FRB 180916.J0158+65 (on MJDs 58410, 58720 and 58836) each consist of two sub-bursts that occur widely separated in time, with no emission observed between them. In such cases it is unclear whether these pairs of bursts belong to the same envelope emitted by the source, or if they instead represent distinct moments of source activity. Given this ambiguity, we here consider them to be separate bursts. Therefore, although we report on the 10 events registered previously by the CHIME/FRB instrument, we here consider the event on MJD 58410 to be two bursts, and therefore report values for 11 bursts in Extended Data Table 1.

The flux calibration method of the bursts is nearly identical to that previously presented, with one crucial difference. Previously we assumed that each burst was detected along the meridian of the primary beam, at the peak sensitivity of its declination arc. Under this assumption, we calibrated using meridian transit observations of bright sources near the declination of each burst to obtain lower-bound fluences and fluxes. For the current analysis, we instead leverage the precise localization of FRB 180916.J0158.6 combined with our beam model to scale the fluences and fluxes and obtain more accurate values. From the beam model, we determine a per-frequency scaling between the location of the calibrator at the time of transit and the location of the FRB at the time of burst occurrence. We apply this scaling to the calibrated dynamic spectrum of each burst before generating the band-averaged time series from which the fluence and flux are calculated. If there were multiple sub-bursts in a given burst, then separate fluences and fluxes were obtained for each component.

We use this method to calculate fluences and peak fluxes for all FRB 180916.J0158.6 bursts detected by CHIME/FRB, including recalculations for the 11 previously published bursts. More specifically, for each burst located within the FWHM (at 600 MHz) of the synthesized beam in which it was detected, we complete the scaling analysis using the precise position. For all other bursts, we use the method previously presented to obtain lower bounds. For each calculation, we use meridian transit observations of the supernova remnant SNR G130.7+03.1, which is located within 1° in declination from FRB 180916.J0158.6. Fluences and peak fluxes for all bursts are listed in Extended Data Table 1. For bursts within the beam FWHM, fluences calculated using the precise position are on average around 40% larger than the corresponding lower bounds calculated assuming detection along the meridian.

Including both newly and previously detected bursts, but omitting those for which only lower bounds could be calculated, we obtain a population of fluences for 25 FRB 180916.J0158.6 bursts, or a total of 33 sub-bursts. The cumulative distribution function of the 33 sub-burst fluences ($N(>F) \propto F^{\alpha+1}$, where N is the number of bursts detected above a fluence of F) is shown in Extended Data Fig. 4. We determine the power-law index, α, of the differential distribution ($\mathrm{d}N/\mathrm{d}F \propto F^{\alpha}$) using maximum-likelihood estimation methods[36,37]. The turnover in the distribution at lower fluences could be due to our telescope sensitivity limit or the intrinsic burst distribution. To remain agnostic about the cause of the turnover, we pick a fluence threshold that minimizes the Kolmogorov–Smirnov distance between an estimated power law and the underlying distribution. The resulting 5.3 Jy ms threshold is shown in Extended Data Fig. 4 as a black dashed vertical line and our 5.2 Jy ms active period 90% confidence completeness threshold is shown as a blue dash-dotted line. Excluding bursts below the Kolmogorov–Smirnov threshold, we performed a Monte Carlo simulation that resamples the fluences according to their uncertainties to obtain a distribution of estimated power-law indices determined using a maximum-likelihood estimator at each resampling. The mean of the resulting distribution is $\alpha = -2.3 \pm 0.3 \pm 0.1$, where the first error is the statistical uncertainty from the maximum-likelihood estimator and the second error is the standard deviation of the index distribution. This value is consistent with previous results[7], which found that the cumulative distribution of energies from FRB 121102 bursts (detected at 1.4 GHz using the 305-m William E. Gordon Telescope at the Arecibo Observatory) followed a power law with $\gamma = -1.8 \pm 0.3$ (equivalent to a differential distribution index of $\alpha = \gamma - 1 = -2.8$). Both of these values are steeper than the $\alpha \approx -1.7$ that was determined using separate samples of FRB 121102 bursts detected by the Karl G. Jansky Very Large Array at 3 GHz, the Green Bank Telescope at 2 GHz, and the 305-m William E. Gordon Telescope at the Arecibo Observatory at 1.4 GHz (ref. [38]).

Although the comparison of these values is potentially interesting, we reiterate that all are almost certainly contaminated by instrumental biases and probably do not faithfully reflect the underlying source distributions. More robust conclusions about the intrinsic source luminosity function must wait until our CHIME/FRB detection biases are properly evaluated.

Statistical significance of the period

To search for the period, we fold the burst arrival times with different periods, and group the folded bursts into n phase bins. The folding and grouping of the arrival times make the search relatively insensitive to randomly occurring gaps in the data as long as the exposure

is reasonably uniform across phase bins. We then perform the classic Pearson χ^2 test for deviation from uniformity:

$$\chi^2 = \sum_{i=1}^{n} \frac{(N_i - E_i)^2}{E_i}, \quad (1)$$

where n is the total number of phase bins, N_i is the observed number of bursts in bin i, $E_i = pT_i$ is the expected number of bursts from a uniform distribution, T_i the exposure time for bin i, and $p = \sum N_i / \sum T_i$ the average burst rate per unit exposure time. In the case of uniformity, the calculated χ^2 statistic for different folding periods should follow a χ^2 distribution with $n-1$ degrees of freedom (DOF) in the limit as $N \to \infty$. A reduced $\chi^2 \gg 1$ indicates a periodicity unlikely to arise by chance. In the study of FRBs, owing to the limited sample size, the large-N limit may not hold. Then the likelihood of a set of phase bin counts N_i will follow the discrete multinomial distribution:

$$P(\{N_i\}) = \frac{N!}{\prod_{i=1}^{n} N_i!} \prod_{i=1}^{n} p_i, \quad (2)$$

where $N = \sum N_i$ is the total number of bursts; $p_i = E_i/N$ is the expected chance of falling into phase bin i; and n is again the total number of phase bins. The chance of coincidence with a set of phase bin counts N_i observed corresponds to the sum of the likelihood of all possible permutations N_k that have the same or less likelihood as $P(\{N_i\})$. We verify the statistical significance of any detected periodicity with the chance of coincidence from multinomial distribution.

We searched for periods from $P_{\rm min} = 1.5$ d to $P_{\rm max} = 100$ d in steps of $0.1/T$ in frequency (that is, inverse of the period) space, where $T = 506$ d is the longest separation between burst arrival times. We currently only search for periods of days, as opposed to smaller timescales, to avoid the complexity introduced by the cadence of the source transiting CHIME at a sidereal day and the beam response of CHIME during the daily exposure. Moreover, the number of independent periods that need to be searched is proportional to $1/P$, so the 'look elsewhere' effect would be orders of magnitude larger for searches with short periodicity, leading to periodicities arising by chance. $P_{\rm min}$ is chosen to be sufficiently larger than a sidereal day such that the modulation of the Fourier spectrum from the sidereal day fades away, and $P_{\rm max}$ is chosen so that the extent of the observation time consists of enough cycles. We limit our search to a period of $P_{\rm max} = 100$ d, to ensure at least five cycles during the time extent. This is because 'phantom periodicity' could arise in non-Poisson stochastic process, but typically only for fewer than three cycles[39]. There is a strong instrumental periodicity at a sidereal day owing to the cadence of the source transiting CHIME, so we avoid searching periods close to the first five subharmonics of a sidereal day, $P^N_{\rm sid} = NP_{\rm sid}$, with $P_{\rm sid} = 0.99727$ d and N an integer. Given the longest separation between burst arrival times T, periods with $|1/P - 1/P^N| < 0.2/T$ are ignored in the search for N between 1 and 5.

After calculating χ^2 against the folding period, we noticed a distinct peak at $P = 16.35 \pm 0.15$ d, which persists for searches using 4, 8 and 16 phase bins. We estimate the significance with five phase bins, so that the bin size corresponds to the FWHM of the profile folded at 16.35 d. The reduced $\chi^2 = 31.7$, with five phase bins (four DOFs). This corresponds to a probability of chance coincidence of about 10^{-23} (equivalent to 10σ) after taking into consideration the number of independent trials searched, $N_{\rm ind} = (1/P_{\rm min} - 1/P_{\rm max})T \approx 332$. The chance of coincidence from the multinomial distribution is 10^{-20} (9.2σ), after multiplying the number of independent trials searched. The period uncertainty is conservatively estimated by $\sigma_P = PW_{\rm active}/T_{\rm span}$, where P is the period, $W_{\rm active}$ is the active days in the period and $T_{\rm span}$ is the longest time separation between burst arrival times. This corresponds to a change in period that would allow the folded pulse to drift across the active cycle over the observed time span. The calculated error also corresponds to the FWHM of the peak in the periodogram. The period and error are reported at an accuracy of 0.05 d. Within this accuracy, all the following approaches return consistent results.

The above analysis shows that there is a significant 16.35-d periodicity in the arrival times of FRB 180916.J0158+65 assuming that all the bursts are independent events (Poisson statistics). However, for the first repeater, FRB 121102, in which no periodicity has yet been found, the bursts are observed to be clustered[8]. This triggers the concern that the arrival times of nearby bursts in FRB 180916.J0158+65 may not be independent. Correlated processes have been shown to contaminate the significance of apparent periodicities in certain contexts[39]. To mitigate this effect, we apply the search assuming different correlation lengths. The CHIME daily exposure is only tens of minutes; stochastic processes with a correlation timescale smaller than 10 min should not introduce a periodicity at tens of days. Also, stochastic processes with a correlation timescale longer than 16 d cannot account for 50% of the bursts appearing in a 0.6-d window. Therefore, two crucial correlation timescales to consider are 0.6 d, the size of the peak active window, and 5 d, the size of the active phase.

First, we assume a correlation timescale of 0.6-d for the detected bursts. Then all the bursts detected in the tens of minutes of exposure of one sidereal day are correlated events. We assign a total weight of unity to bursts that arrived on the same sidereal day. After weighting, there are 23 active dates, for the 38 bursts detected by CHIME/FRB. In this way, we also reduce the influence from inaccurate mapping of beam response within the exposure of a sidereal day.

After weighting the events, the distinct peak at 16.35 d persists in the χ^2 against folding periods, followed by a peak at its harmonic of about 32.7 d. The reduced χ^2 versus period with five phase bins is shown in Fig. 1a. The corresponding chances of the highest peak from the χ^2 distribution is about 10^{-11}, equivalent to 6.8σ, and the significance from the multinomial distribution is 6.1σ. Both approaches have taken into consideration the number of independent trials searched.

Given that the 16.35-d periodicity is not an integer number of sidereal days, the influence of the exposure map on the significance is small. To further exclude the possibility of instrumental periodicity, we applied bootstrap tests to the mock burst arrival times randomly sampled according to the daily exposure to FRB 180916.J0158+65 within the FWHM of the synthesized beams of CHIME/FRB at 600 MHz, as well as to a random selection of single bursts from Galactic radio pulsars at similar declinations and detected by CHIME/FRB. The mock exposure samples are chosen from the exposures between 28 August 2018 to 30 September 2019 (about 80% of the total time span); several upgrades were made to the CHIME/FRB detection pipeline after October 2019 making characterization of the exposure and sensitivity variation difficult. 26 out of the total 38 bursts (occurring on 17 of 23 active days and during 10 of 14 active cycles) are detected during this time span and the 16.35-d periodicity is already manifest with this fraction of data. Therefore, if there are instrumental effects leading to the periodicity, we expect it to appear in the mock samples as well. An example of the reduced χ^2 versus period from two sets of the random samples with the same number of active days as FRB 180916.J0158+65 is shown in Fig. 1b (random sample selected according to the exposure map) and Fig. 1c (random samples from the detection of PSR B2319+60). With 10^6 sets of random samples from the exposure map, and 10^6 sets each from PSR B2319+60, B0138+59, B2224+65, we have not found any period unrelated to sidereal day that has reached the level of significance of the 16.35-d period for FRB 180916.J0158+65.

In a conservative approach, we assume all the bursts arriving in the active phase of the same cycle are clustered owing to mechanisms irrelevant to the periodicity. We assign a total weight of unity for bursts with separation less than 5 d and search for periods. The 16.35-d periodicity is still the most prominent peak, with a significance of 4.5σ from a χ^2 distribution, and 4.2σ from a multinomial distribution after taking into account the number of trials searched. (We note that the multinomial distribution deals with discrete events only, so we treated clustered

pulses by repeatedly drawing one random pulse from each cluster group, and we report the average probability of many trials.)

For any other correlation timescale assumed, its influence on the significance would be less strong than this one. Therefore, we conclude that the periodicity is significant even after taking into account potential clustering.

We also performed a H test[12], summing over N harmonics with N varying from 1 to 10, and discrete Fourier transform searches with incoherent harmonic summing[13] on the arrival times of FRB 180916.J0158+65. With all these approaches, with or without subtracting the exposure map, with different weighting, the roughly 16.35 ± 0.15-d period remains prominent, and the significance varies between 5–13σ. No other statistically significant periods (other than those harmonically related to this approximately 16-d period) appear in the searched range.

Although owing to our incomplete knowledge of the underlying burst distribution the definite value of the significance of the observed periodicity is undetermined, the periodicity is evident with all the approaches we have tried, and does not exist in any of the control samples. We did not find a phase evolution with time. Therefore, we conclude that the periodicity of FRB 180916.J0158+65 is statistically significant and astrophysical in origin.

Aliasing due to limited daily exposure

The short regular daily exposure of CHIME could lead to a degeneracy between frequency $f_0 = (P_0)^{-1} = (16.35\ \mathrm{d})^{-1}$ and an alias $f_N = Nf_{\mathrm{sid}} \pm f_0$, where N is an integer and $f_{\mathrm{sid}} = (0.99727\ \mathrm{d})^{-1}$ is the frequency of a sidereal day. An upper limit on N can be estimated using the observed duty cycle (D) over exposure time—that is, the duty cycle of the intrinsic period should be longer than the exposure time. With the observed 16.35-d period, all bursts arrive in a 5-d phase window. With 12 min (that is, 0.008 sidereal days) daily exposure, the upper limit on N is $5/16.35/0.008 \approx 37$. However, 50% of the CHIME bursts are detected in a 0.6-d phase window, with the event rate dropping rapidly towards the edges of the active phase. If 0.6 d is the width of the active phase, the duty cycle is 0.04, and $N > 5$ would be disfavoured. We slightly favour $N = 0$ for several reasons: (1) If there is aliasing, the observed frequency f_0 should be randomly distributed between 0 and 0.5 d^{-1}. However, $f_0 = (16.35\ \mathrm{d})^{-1} = 0.06\ \mathrm{d}^{-1}$ is on the low side of that range, which seems slightly fine-tuned (the chance to obtain $f_0 \leq 0.06$ has a P value of 0.06/0.5 = 0.12); (2) If we define the duty cycle D to be the fractional phase that contains half of the events, then $N = 0$ has the smallest $D = 0.036$, followed by $N = 1$, $D = 0.044$, with larger D for higher N; (3) For most physical models, we expect the bursts detected in the 1.7-GHz EVN observations to have the same periodicity, with alignment of epochs of activity; only periods of 16.35 d ($N = 0$), 0.20 d ($N = 5$) and 0.14 d ($N = 7$) satisfy this condition. But the duty cycles of the latter two periods are twice as wide as the 16.35-d period. Despite those arguments to favour $N = 0$, or a periodicity of 16.35-d, we cannot unambiguously rule out other values of N with current data. Nevertheless, a statistically significant astrophysical periodicity must exist for aliasing to happen. The exposure of CHIME, as a transit telescope, is fixed by design and therefore we cannot rule out aliased periods with CHIME/FRB detections alone. However, a modest amount of exposure in the same band using other telescopes, with bursts detected outside the CHIME observing windows, may be able to determine the true period.

Exposure and fluence completeness determination

The exposure to the EVN position[10] for the source was calculated by summing the duration of daily transits across the FWHM region of the synthesized beams of the CHIME/FRB system at 600 MHz. After excluding transits for which the observations were interrupted by pipeline upgrades and testing, we estimate the total exposure to be 64 h in the interval from 28 August 2018 to 30 September 2019. We report exposure up to 30 September 2019 because several upgrades were made to the CHIME/FRB detection pipeline throughout October 2019, making characterization of the exposure and sensitivity variation difficult. The increased exposure time for several days in February 2019 is due to the occurrence of two transits in the same UTC day caused by the differing lengths of a solar and a sidereal day (see Fig. 2).

The burst activity is not constant within the active phase (see Fig. 3c), and so we divide the active phase into three subintervals to derive estimates of the exposure and detection rate. The first of these subintervals is a ±0.9-d span (standard deviation in the phases derived by folding burst arrival times) centred on the epoch of peak activity. The detection rate estimated for this subinterval is $1.8^{+1.3}_{-0.8}$ bursts per hour above a fluence threshold of 5.2 Jy ms, on the basis of 13 of the 38 detections. The second subinterval is defined as the duration between 1σ and 2σ (that is, between 0.9 and 1.8 d) of the epoch of peak activity; the third subinterval starts at 2σ and covers the remaining active phase. The detection rate in the second subinterval is $0.8^{+1.0}_{-0.5}$ bursts per hour, and that in the third is $0.1^{+0.6}_{-0.1}$ bursts per hour, with five and one detections in these two subintervals, respectively. The rate in the first subinterval is inconsistent with that in the third, hinting at a variation of burst rate within the active phase. Poissonian uncertainties associated with all rate measurements are at the 95% confidence level, and the fluence thresholds are complete to the 90% confidence level.

The variability of the event rate within the active phase can influence the chance of detection in different cycles. 50% of the bursts are detected in a narrow 0.6-d phase window. CHIME only has tens of minutes of exposure per sidereal day. Therefore, for 40% of the observed cycle, the 0.6-d peak activity window lies outside of the CHIME exposure window, which reduces the chance of detection. This effect will be better studied when more bursts are collected and the event rate versus phase can be better modelled.

The CHIME/FRB system operated nominally for a total of 21 h in the active phases, defined as a ±2.7-d interval around each epoch of source activity. 19 of the 38 detections occurred during intervals included in this exposure time. A total of 7 h of the exposure was within a ±0.9-d interval of estimated epochs of peak source activity, with 13 out of the 38 reported bursts detected in this period. The other 25 bursts were not included in the calculation of the detection rate for various reasons: six of these bursts were emitted outside the fiducial definition of the active phase, 12 were detected after the interval used for the evaluation of the exposure, six were detected when the source location was not within the FWHM region of the synthesized beams at 600 MHz and one was detected on 16 September 2018 when system metrics were not being recorded by the detection pipeline. The other two subintervals had an exposure of 7 h each. The exposure in the inactive phase (outside the ±2.7-d intervals around the estimated epochs of activity for the source) was a total of 43 h.

To characterize the variation in sensitivity (due to changes in gain calibration, the detection pipeline and radio-frequency interference (RFI) environment) for each day included in the exposure, we use a method described previously[15]. We analyse the distribution of the value of S/N for pulsars detected with CHIME/FRB within 10° of the source declination. In contrast to the previous approach, we use pulsars that were detected on each sidereal day for which the telescope was operating with the same gain calibration, instead of within a UTC day. For each pulsar, the r.m.s. noise is measured relative to the median over all days the pulsar was detected. A weighted average of these measurements for all pulsars provides an estimate of the overall variation in r.m.s. noise on each sidereal day.

Fluence completeness was determined following previously reported methods[4,15]. These methods consider sensitivity variation owing to observing epoch, position along transit, and burst spectral shape. In a Monte Carlo simulation with 10^6 realizations, fluence detection thresholds for different scenarios are generated for a given period of exposure. These simulations produce a set of relative sensitivities that are tied to a flux scale using bandpass-calibrated observations. Owing to the structured nature of both bandpass and transit sensitivity, the

final distribution of fluence thresholds is non-Gaussian. Therefore, we take percentiles of the distribution to quote completeness at a given confidence level. We use the bursts reported in Extended Data Table 1 as reference observations to simulate fluence thresholds for both the active and inactive periods, finding completeness at the 90% confidence interval of 5.2 Jy ms and 5.1 Jy ms, respectively.

Effelsberg observations and analysis

Motivated by the detection of the 16.35-d period, we observed FRB 180916.J0158+65 at 1.4 GHz using the 100-m Effelsberg radio telescope and PSRIX data recorder[40] for 17.6 h during a predicted active period (29 October 2019 and 30 October 2019). Details of the scan start times and durations are shown in Extended Data Table 2. We observed with a total bandwidth of 250 MHz, from 1,234 MHz to 1,484 MHz, divided into 2,048 channels. The data were recorded with time and frequency resolutions of 131.072 μs and 0.122 MHz, respectively.

The high-time-resolution data were analysed in the search for millisecond-duration radio bursts, using tools from the PRESTO suite of pulsar software[41]. The data were first searched for RFI, and the contaminated frequency channels and time intervals were masked using the tool *rfifind*. Dedispersed time series were generated for the DM range 300–400 pc cm^{-3} in steps of 0.3 pc cm^{-3} using the tool *prepdata*. We searched each dedispersed time series for single pulses using *single_pulse_search.py*. The single pulses identified were filtered for RFI in the search for astrophysical bursts, above a 7σ threshold, using an automated classifier[42,43]. Given the frequency resolution of the PSRIX data, the intra-channel smearing is around 0.15 ms at the DM of FRB 180916.J0158+65. This is comparable to the time resolution of the data. Our search was sensitive up to burst widths of 39.3 ms. Bursts from FRB 180916.J0158+65 have been observed[10] with components as narrow as roughly 60 μs. Therefore, it is possible that FRB 180916.J0158+65 is producing weak, narrow bursts to which this search was not sensitive.

In this search we did not detect any bursts from FRB 180916.J0158+65 above a 7σ threshold. By taking typical values of the system temperature and gain for the Effelsberg telescope (T_{sys} = 20 K, G = 1.54 K Jy^{-1}), estimating a background temperature of 5 K using the 408 MHz all-sky map[44] and extrapolating to 1.4 GHz using a spectral index[45] of −2.7, we use the radiometer equation to derive the fluence limit of our search (following previous work[46]). Assuming a burst width of 1 ms and a minimum S/N of 7, we were sensitive to bursts from FRB 180916.J0158+65 above a fluence threshold of 0.17 Jy ms.

Interestingly, during this predicted active epoch of FRB 180916.J0158+65, two bursts with a fluence exceeding 2 Jy ms, were detected by CHIME/FRB (Extended Data Table 1). The times of arrival of both bursts are within the same Effelsberg telescope scan indicated in Extended Data Table 2. Given our detection threshold of 0.17 Jy ms, if these bursts were equally bright at 1.4 GHz, our search should have been sufficiently sensitive to detect them. The spectra of the two CHIME/FRB bursts peak in the lower half of the 400–800-MHz band. The detection of bursts with CHIME/FRB and the contemporaneous non-detection with the Effelsberg telescope suggests that observed activity from FRB 180916.J0158+65 depends on frequency. In addition, the previously detected bursts from FRB 180916.J0158+65 with the EVN at 1.7 GHz are found at the leading edge of the activity cycle observed at 400–800 MHz (Fig. 3). Future multi-frequency observations of FRB 180916.J0158+65 during predicted active periods are crucial to quantify this behaviour.

Data and code availability

The data and code used in this publication are available at https://chime-frb-open-data.github.io (https://doi.org/10.11570/20.0002).

34. Michilli, D. DM_phase (2019); https://github.com/danielemichilli/DM_phase.
35. The CHIME/FRB Collaboration. Observations of fast radio bursts at frequencies down to 400 megahertz. *Nature* **566**, 230–234 (2019).
36. Clauset, A., Shalizi, C. R. & Newman, M. E. J. Power-law distributions in empirical data. *SIAM Rev.* **51**, 661–703 (2009).
37. Alstott, J., Bullmore, E. & Plenz, D. powerlaw: a Python package for analysis of heavy-tailed distributions. *PLoS One* **9**, e85777 (2014); correction **9**, e95816 (2014).
38. Law, C. J. et al. A multi-telescope campaign on FRB 121102: implications for the FRB population. *Astrophys. J.* **850**, 76 (2017).
39. Vaughan, S. et al. False periodicities in quasar time-domain surveys. *Mon. Not. R. Astron. Soc.* **461**, 3145–3152 (2016).
40. Lazarus, P. et al. Prospects for high-precision pulsar timing with the new Effelsberg PSRIX backend. *Mon. Not. R. Astron. Soc.* **458**, 868–880 (2016).
41. Ransom, S. M. *New Search Techniques for Binary Pulsars*. PhD thesis, Harvard Univ. (2001).
42. Michilli, D. et al. Single-pulse classifier for the LOFAR Tied-Array All-sky Survey. *Mon. Not. R. Astron. Soc.* **480**, 3457–3467 (2018).
43. Michilli, D. & Hessels, J. W. T. SpS: Single-pulse Searcher (2018); https://github.com/danielemichilli/SpSy.
44. Remazeilles, M., Dickinson, C., Banday, A. J. & Bigot-Sazy, M.-A. & Ghosh, T. An improved source-subtracted and destriped 408-MHz all-sky map. *Mon. Not. R. Astron. Soc.* **451**, 4311–4327 (2015).
45. Reich, P. & Reich, W. A map of spectral indices of the galactic radio continuum emission between 408 MHz and 1420 MHz for the entire northern sky. *Astron. Astrophys. Suppl. Ser.* **74**, 7–23 (1988).
46. Cordes, J. M. & McLaughlin, M. A. Searches for fast radio transients. *Astrophys. J.* **596**, 1142–1154 (2003).

Acknowledgements We thank the Dominion Radio Astrophysical Observatory, operated by the National Research Council Canada, for hospitality and expertise. The CHIME/FRB Project is funded by a grant from the Canada Foundation for Innovation 2015 Innovation Fund (project 33213), as well as by the Provinces of British Columbia and Québec, and by the Dunlap Institute for Astronomy and Astrophysics at the University of Toronto. Additional support was provided by the Canadian Institute for Advanced Research (CIFAR), McGill University and the McGill Space Institute via the Trottier Family Foundation, and the University of British Columbia. Research at Perimeter Institute is supported by the Government of Canada through Innovation, Science and Economic Development Canada and by the Province of Ontario through the Ontario Ministry of Economic Development, Job Creation and Trade. The National Radio Astronomy Observatory is a facility of the National Science Foundation (NSF) operated under cooperative agreement by Associated Universities, Inc. FRB research at the University of British Columbia is supported by an NSERC Discovery Grant and by the Canadian Institute for Advanced Research. The CHIME/FRB baseband system is funded in part by a CFI John R. Evans Leaders Fund grant to I.H.S. The Dunlap Institute is funded through an endowment established by the David Dunlap family and the University of Toronto. A.S.H. was partly supported by the Dunlap Institute at the University of Toronto. B.M. acknowledges support from the Spanish Ministerio de Economía y Competitividad (MINECO) under grants AYA2016-76012-C3-1-P and MDM-2014-0369 of ICCUB (Unidad de Excelencia 'María de Maeztu'). B.M.G. acknowledges the support of the Natural Sciences and Engineering Research Council of Canada (NSERC) through grant RGPIN-2015-05948, and of the Canada Research Chairs programme. D.M. is a Banting Fellow. M.B. is supported by a Fonds de recherche du Québec – Nature et technologies (FRQNT) Doctoral Research Award. M.D. is supported by a Killam Fellowship and receives support from an NSERC Discovery Grant, CIFAR, and from the FRQNT Centre de Recherche en Astrophysique du Québec. P.C. is supported by an FRQNT Doctoral Research Award. P.S. is a Dunlap Fellow and an NSERC Postdoctoral Fellow. S.M.R. is a CIFAR Fellow and is supported by the NSF Physics Frontiers Center award 1430284. U.-L.P. receives support from the Ontario Research Fund – Research Excellence (ORF-RE) programme, the Natural Sciences and Engineering Research Council of Canada (NSERC), the Simons Foundation, Thoth Technology Inc. and the Alexander von Humboldt Foundation. V.M.K. holds the Lorne Trottier Chair in Astrophysics and Cosmology and a Canada Research Chair and receives support from an NSERC Discovery Grant and Herzberg Award, from an R. Howard Webster Foundation Fellowship from the Canadian Institute for Advanced Research (CIFAR), and from the FRQNT Centre de Recherche en Astrophysique du Québec. Z.P. is supported by a Schulich Graduate Fellowship. F.K. acknowledges support by the Swedish Research Council. J.W.K. is supported by NSF OIA Award 1458952. The European VLBI Network is a joint facility of independent European, African, Asian and North American radio astronomy institutes. Scientific results from EVN data presented in this publication are derived from the following EVN project code: EM135. This work is based in part on observations with the 100-m telescope of the MPIfR (Max-Planck-Institut für Radioastronomie) at Effelsberg. We thank L. Spitler, M. Cruces and M. Kramer for their help in acquiring Effelsberg observing time. We thank R. Archibald for discussions regarding the H test. We thank S. Chatterjee for pointing out the aliasing possibility to us.

Author contributions All authors from the CHIME/FRB collaboration had either leadership or major supporting roles in one or more of: the management, development and construction of the CHIME telescope, the CHIME/FRB instrument and the CHIME/FRB software data pipeline, the commissioning and operations of the CHIME/FRB instrument, the data analysis and preparation of this manuscript. All authors from the CHIME collaboration had either leadership or major supporting roles in the management, development and construction of the CHIME telescope. K.N., J.W.T.H., B.M., Z.P., A.K., F.K. and R.K. performed the analysis of the EVN and Effelsberg single-dish data.

Competing interests The authors declare no competing interests.

Additional information
Correspondence and requests for materials should be addressed to D.L.

Peer review information *Nature* thanks Vikram Ravi and the other, anonymous, reviewer(s) for their contribution to the peer review of this work.

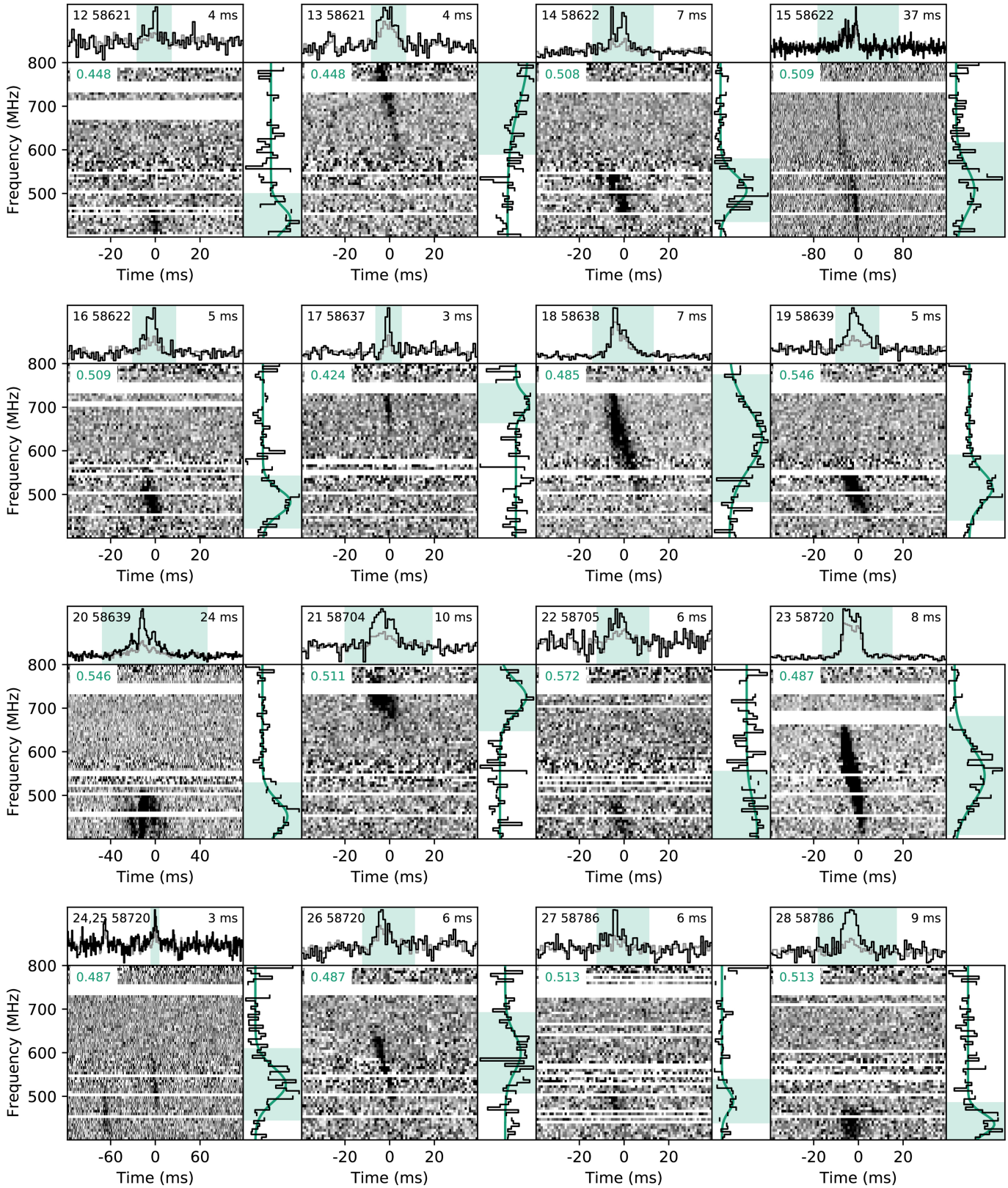

Extended Data Fig. 1 | Dynamic spectra of newly reported bursts (bursts 12–28 in Extended Data Table 1). Bursts with separations of less than 0.1 s are shown in joint spectra (bursts 24 and 25). All bursts are dedispersed to 348.82 pc cm^{-3}. The sequence number of the burst and the arrival date (in MJD) is given in each top-left corner. The arrival phase of the bursts within the 16.35-d cycle is given in the top left corner of each spectrum. Each plot also gives the 0.98304-ms time-resolution dedispersed intensity data with the integrated burst profile on top and the on-pulse spectrum on the right (arbitrary units). Intensity values are saturated at the 5th and 95th percentiles. Pulse widths—defined as the width of the boxcar with the highest *S*/*N* after convolution with the burst profile—are given in the top-right corner. The shaded region in each profile (four times the pulse width) was used for the extraction of the on-pulse spectrum. The shaded region in the on-pulse spectrum shows the full width at tenth maximum of a Gaussian fit. In each burst profile, the black line is the integration over the full width at tenth maximum of the spectrum and the grey line is the integration over the full bandwidth. For better visualization, we downsampled the full-resolution data (16,384 channels) to 64 sub-bands, each with a bandwidth of 6.25 MHz. Horizontal white bands represent missing or masked data. There are underlying missing or masked channels at full resolution, resulting in an average effective bandwidth of 224 MHz.

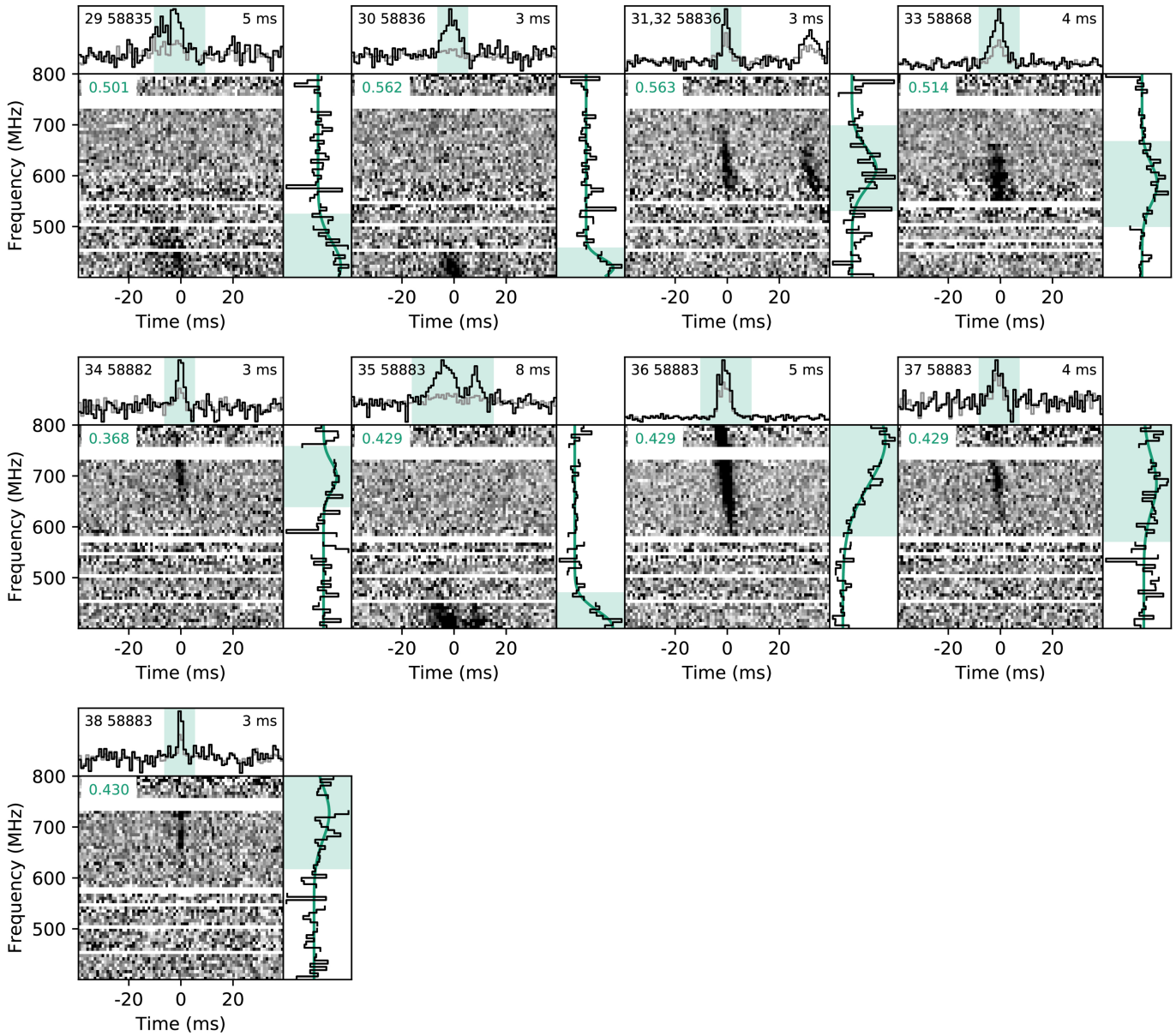

Extended Data Fig. 2 | Dynamic spectra of newly reported bursts (bursts 29–38 in Extended Data Table 1). As in Extended Data Fig. 1. Bursts 31 and 32 are shown in joint spectra.

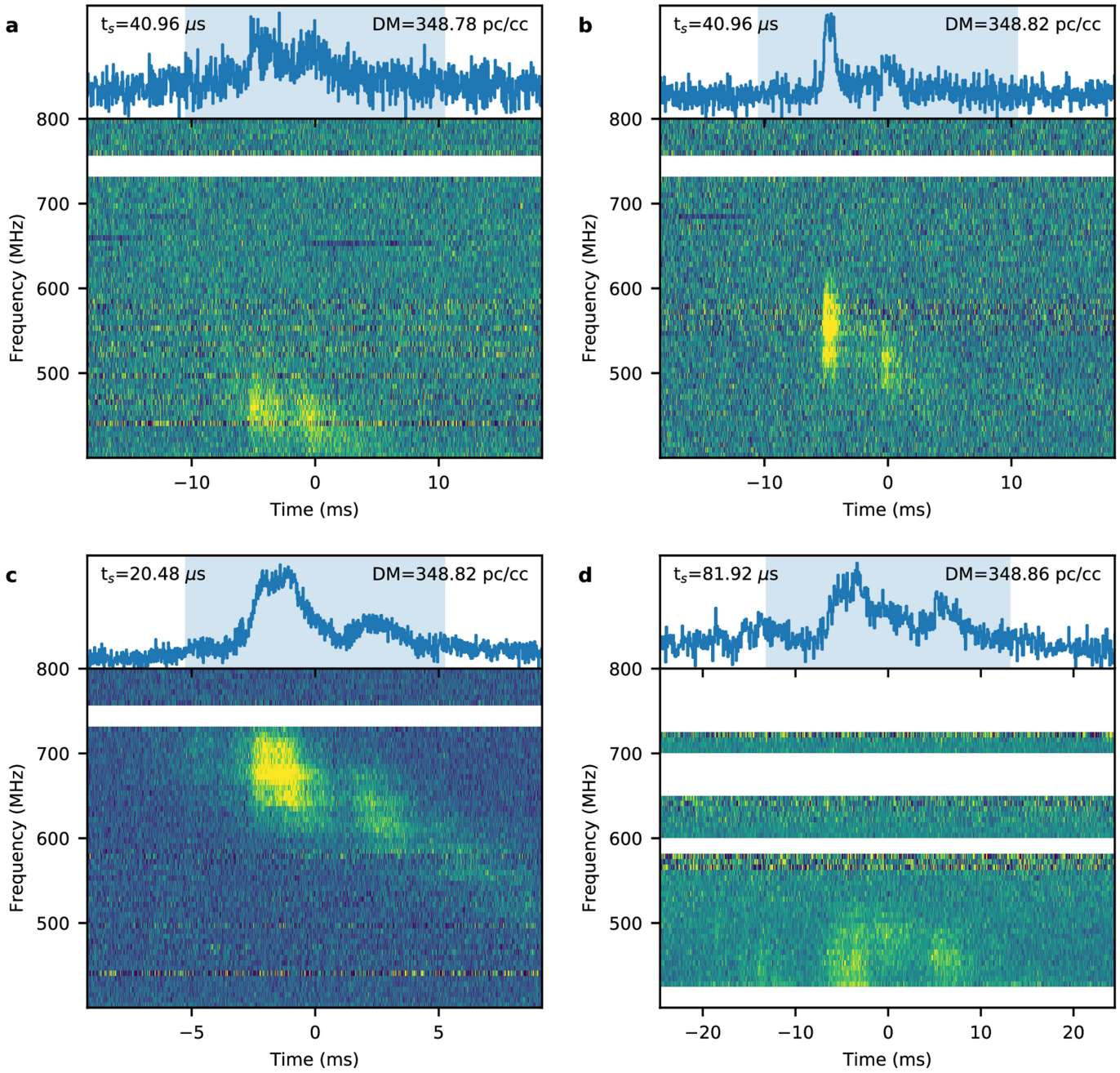

Extended Data Fig. 3 | Dynamic spectra of the bursts with available baseband data. a–d, Bursts 9 (**a**), 10 (**b**), 18 (**c**) and 20 (**d**) (see Extended Data Table 1), dedispersed to their per-burst optimal DM, which is listed in each top-right corner. The sampling time (t_s) after downsampling is listed in each top-left corner. Intensity values are saturated at the 1st and 99th percentiles. 64 frequency sub-bands with a 6.25-MHz sub-band bandwidth are shown for all bursts. Horizontal white bands represent missing or masked data. pc/cc, pc cm^{-3}.

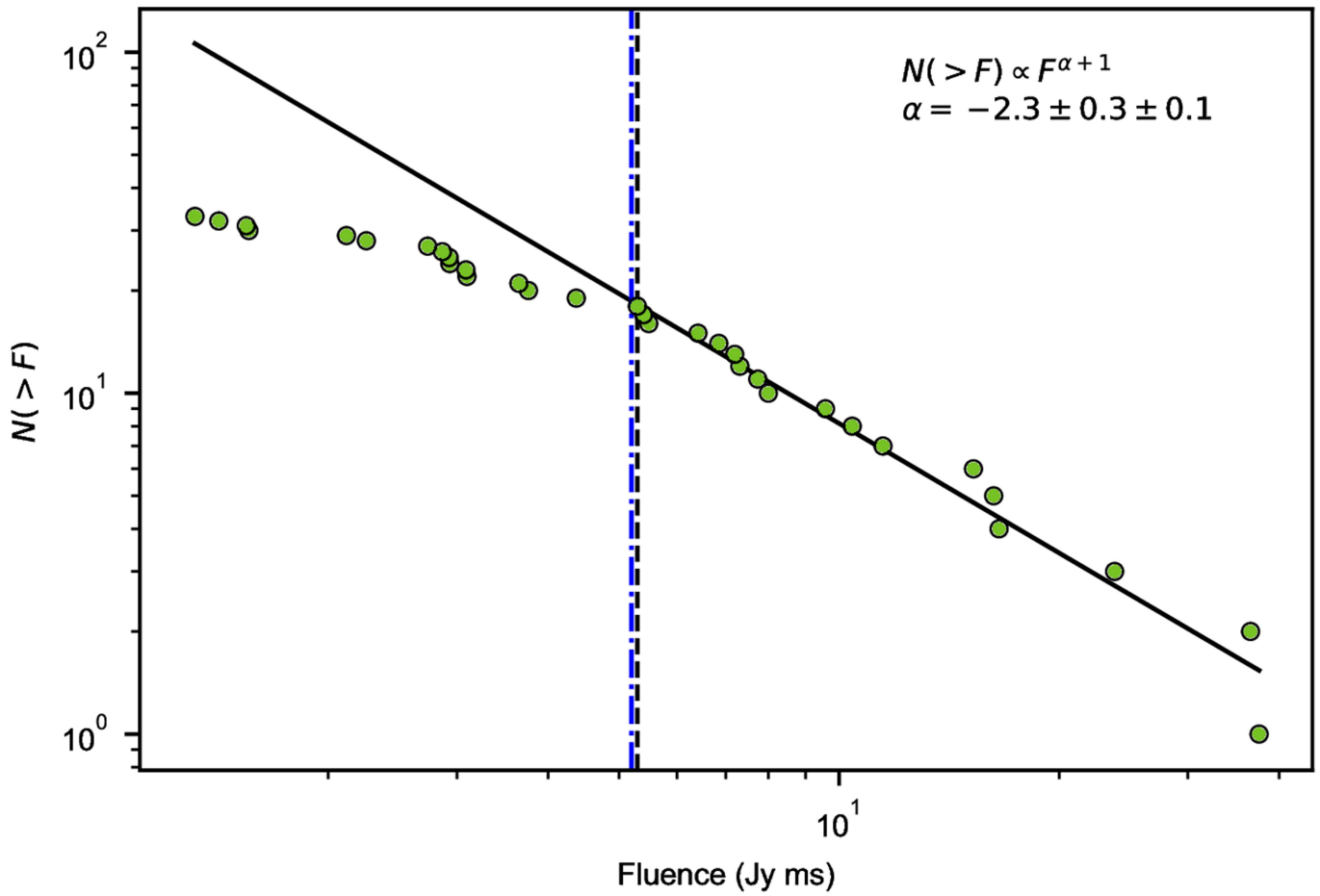

Extended Data Fig. 4 | Cumulative distribution of burst fluences. The distribution is composed of both the newly detected bursts and those previously detected. Excluding bursts detected beyond the 600-MHz FWHM of any CHIME/FRB synthesized beam, this includes 25 bursts split into sub-bursts, yielding 33 fluence measurements. The black solid line represents the maximum-likelihood estimated power law with differential distribution index $\alpha = -2.3 \pm 0.3 \pm 0.1$, where the first error is the statistical uncertainty from the maximum-likelihood estimator and the second error is the standard deviation of the distribution of power-law indices obtained from a Monte Carlo simulation that resamples the fluences according to their uncertainties. The black dashed vertical line denotes the 5.3 Jy ms threshold determined by minimizing the Kolmogorov–Smirnov distance between a power-law fit and the underlying data. The blue dash-dotted vertical line denotes the 5.2 Jy ms active period 90% confidence completeness threshold.

Extended Data Table 1 | Burst properties

	MJD (pc cm^{-3})	DM (ms)	Total Width (Jy ms)	Fluence (Jy)	Peak Flux
			Previously Published Bursts[4]		
1	58377.42972096	349.2±0.2	1.40±0.07	>2.3±1.2	>1.4±0.6
2	58410.34656422*	349.0±0.6	4.1±0.3	>3.5±1.3	>0.6±0.3
3	58410.34656495*	349.0±0.6	4.4±0.9	>2.0±0.8	>0.3±0.2
4	58426.29413444	349.5±0.3	1.37±0.07	>2.8±0.9	>1.4±0.5
5	58426.30088378	349.6±0.2†	6.3±1.1	6.8±3.0	1.0±0.6
6	58442.25174905	349.9±0.6	1.10±0.09	8.0±2.2	2.9±1.1
7	58474.17007574	349.1±0.1	4.95±0.4 / 1.51±0.3 / 3.7±0.3 / 2.8±0.3	9.6±2.6 / 15±4 / 16.5±4.5 / 7.2±1.8	1.9±0.6 / 6.3±1.8 / 3.5±1.0 / 0.9±0.4
8	58475.16454902	349.7±0.7	1.67±0.05 / 6.3±0.4	10.4±2.9 / 3.6±1.5	1.9±0.6 / 0.5±0.3
9	58477.16557196	348.9±0.7‡	3.8±0.3	3.1±2.4	1.4±0.8
10	58478.15889115	348.8±0.8‡	0.87±0.3 / 3.6±0.4	2.9±0.8 / 1.6±0.5	1.9±0.6 / 0.7±0.3
11	58509.06654412	349.8±0.5	2.53±0.13	6.4±1.2	1.7±0.5
			Bursts from This Work		
12	58621.75641235	349.8±0.7†	2.5±0.6	1.0±0.3	0.4±0.2
13	58621.76154355	350.2±0.3	1.96±0.16	7.7±1.8	1.6±0.5
14	58622.74024356	348.9±0.1	0.58±0.08 / 0.9±0.1	>1.3±0.5 / >2.2±0.9	>0.8±0.4 / >0.8±0.5
15	58622.75315853	349.4±0.2	8.0±0.7 / 2.63±0.16	3.1±1.4 / 5.3±2.4	0.9±0.5 / 1.0±0.6
16	58622.75441645	349.3±0.4	3.6±0.4	4.4±2.0	1.1±0.7
17	58637.71187752	349.9±0.5	1.9±0.2	2.1±0.8	1.6±0.8
18	58638.71347350	348.82±0.05‡	1.00±0.05	37±9	6.3±1.9
19	58639.70267121	349.7±0.2	2.34±0.08	>7.0±1.5	>1.3±0.4
20	58639.70713864	348.86±0.5‡	3.72±0.13 / 4.1±0.4	11.5±4.0 / 5.4±2.7	2.3±0.7 / 1.1±0.5
21	58704.53530987	349.6±0.3	3.43±0.14	7.3±1.2	1.2±0.3
22	58705.53461219	349.3±0.9†	4.3±1.6	>1.7±0.3	>0.4±0.2
23	58720.49302597	349.0±0.1	1.83±0.03	24±4	4.9±1.0
24	58720.49551788*	349.7±0.4	7.8±1.3	2.8±0.9	0.6±0.3
25	58720.49551860*	349.7±0.4	5.1±0.8	1.4±0.6	0.5±0.3
26	58720.49669723	349.5±0.5	1.3±0.3	>2.6±0.5	>0.9±0.3
27	58786.31947325	349.7±0.7†	3.1±0.7	2.3±0.8	0.9±0.8
28	58786.32497972	349.1±0.4†	3.6±0.4	>2.3±0.5	>0.5±0.2
29	58835.17721035	349.5±0.5	5.0±0.5	2.9±0.7	0.4±0.2
30	58836.17591788	350.1±0.4	4.2±0.4	1.3±0.3	0.3±0.2
31	58836.17845766*	349.5±0.2	1.55±0.13	2.9±0.9	0.9±0.3
32	58836.17845804*	349.5±0.2	2.9±0.2	3.8±1.0	0.9±0.3
33	58868.07829861	349.6±0.4	2.36±0.10	5.5±1.5	1.0±0.4
34	58882.04838586	349.4±0.3	1.14±0.12	>0.8±0.3	>0.5±0.2
35	58883.04146680	349.6±0.3	8.6±0.5	>4.3±1.6	>0.4±0.3
36	58883.04307123	349.81±0.05	1.157±0.011	16.3±5.0	6.1±2.0
37	58883.04556977	349.8±0.5	1.48±0.13	1.5±0.6	0.5±0.2
38	58883.05523556	348.7±0.6	0.76±0.07	>0.4±0.1	>0.5±0.3

Best-fit parameters for 38 bursts from FRB 180916.J0158+65 detected by CHIME/FRB. Uncertainties are reported at the 68.3% confidence level. Bursts with multiple components have one arrival time and several widths, fluences, and peak fluxes reported; the arrival time refers to the arrival of the first sub-burst from the EVN position at the Solar System barycentre after correcting to infinite frequency (that is, after removing the time delay from dispersion) using the listed DM. Fluence and peak flux values for each sub-burst component are presented in order of arrival.
*Considered to be separate bursts observed during the same CHIME/FRB event owing to large time separation and no clear emission between bursts. See Methods section 'Burst characterization' for a brief discussion.
†From *S*/*N* optimization.
‡From structure optimization of CHIME/FRB baseband data.

Extended Data Table 2 | Effelsberg observations

	Scan time range (date time UTC)	Scan time range* (MJD)	Duration (s)
	2019 Oct 29 22:16:20 – 2019 Oct 30 00:16:06	58785.93233 – 58786.01550	7186
	2019 Oct 30 00:18:40 – 2019 Oct 30 02:18:23	58786.01728 – 58786.10043	7183
	2019 Oct 30 02:20:50 – 2019 Oct 30 04:20:39	58786.10212 – 58786.18534	7190
	2019 Oct 30 04:23:10 – 2019 Oct 30 06:22:58	58786.18708 – 58786.27027	7188
†	2019 Oct 30 06:25:30 – 2019 Oct 30 08:25:14	58786.27203 – 58786.35519	7184
	2019 Oct 30 08:39:30 – 2019 Oct 30 10:39:18	58786.36509 – 58786.44829	7188
	2019 Oct 30 10:41:50 – 2019 Oct 30 10:58:53	58786.45005 – 58786.46189	1023
	2019 Oct 30 19:33:40 – 2019 Oct 30 21:33:27	58786.81938 – 58786.90257	7187
	2019 Oct 30 21:36:00 – 2019 Oct 30 23:35:44	58786.90434 – 58786.98749	7184
	2019 Oct 30 23:38:10 – 2019 Oct 31 01:00:04	58786.98918 – 58787.04606	4914

Details of the observations of FRB 180916.J0158+65 using the 100-m Effelsberg telescope on 29 October 2019 and 30 October 2019.

*Times quoted at the Solar System barycentre after correcting to infinite frequency (that is, after removing the time delay from dispersion) using a DM of 348.76 pc cm^{-3}.

†Two bursts were detected by CHIME/FRB during this scan.